

Recent Advances in Hypersonic Aerothermodynamics for RLV/TPS Design and Analysis⁺

P.C. Chen, D.D. Liu, L. Tang,
K.T. Chang, and X.W. Gao
ZONA Technology*, Scottsdale, AZ, www.zonatech.com

Introduction

For hypersonics and space access, the National Aerospace Initiative (NAI) goals are: (i) Hypersonics- flight demonstrate increasing Mach number capability each year, reaching Mach 12 by 2012; (ii) Space Access – demonstrate technologies that will drastically increase space access and reliability while decreasing cost. In response to these initiatives, needed technologies were identified by NASA/DoD, to support safe but cost effective launch and recoverable systems. To this end, integrated software development in aerothermodynamics, aerothermoelasticity, thermal protection systems (TPS) and multidisciplinary design optimization (MDO) for RLV in extreme environment are among the urgent enabling technologies.

With ongoing supports of several government agencies, together with our in-house R&D resources, we have been gradually building up a Hypersonic Aerodynamics/Aerothermodynamics for TPS (HYAAT) software system whose capability now ranges from RLV/TPS to space-access vehicle for their design/analysis. The HYAAT system was initiated by a continuing AFRL contractual support [1], its progress and development has been reported in [2, 3, 4]. The purpose of this paper is to report our recent advances made of the HYAAT system. The HYAAT system consists of 4 major modules (see Fig. 1). These include: the Aerodynamics/Aerothermodynamics module, the TPS sizing module, the ASTROS module, and the Trajectory module. Here we will confine our reporting only to the progress of the first two modules, since they are the central pieces in the present R&D efforts.

The aerodynamics/aerothermodynamics module has been generalized from a lower-hierarchy Panel method approach, ZONAIR [5] to include several higher hierarchy CFD approaches consisting of DSMC, Boltzmann/BGK, Navier-Stokes, Euler and Proper Orthogonal Decomposition (POD) flow solvers. The HYAAT road maps due to the latter are shown in Fig 2. The TPS sizing module using the NASA supported MINIVER has been improved to add-in an automated optimization scheme for TPS weight minimization while satisfying all aerothermal and structural constraints. In what follows we will go into the specifics of these two improved modules. Whenever appropriate, applications to basic configurations and several hypersonic flight vehicles will be presented to demonstrate the validity of the HYAAT methodology.

Aerodynamics/Aerothermodynamics Module

The earlier module presented in Fig 1 involves ZONAIR as aerodynamics module and it is coupled with the Aerothermodynamic module using a modified SHABP. Here the improved module presented in Fig 2 replaced this module with high-level CFD methods using the POD technique. Current R&D in this is a part of a grand plan to integrate ZONAIR and the high-level CFD methods into a Computational Fluid/Aero-thermodynamics Software Toolbox (CFAST). The integrated toolbox is presented as a Pyramid as shown in Fig 3.

CFAST Pyramid

This pyramid structure (Fig 3) consists of two fluid dynamics approaches (layers): the Gas-kinetic and the Continuum. The gas-kinetic approach (layer) consists of the microscopic solvers of DSMC (Direct Simulation Monte Carlo), the Boltzmann equation and the so-called BGK approximation [6]. The continuum approach (layer) contains all the macroscopic solvers from RANS (Reynolds averaged Navier-Stokes) to potential flow (e.g., CFL3D [7] to ZONAIR [5]). The left-hand face of the pyramid lists the aerodynamic methods whereas the right-hand face the aerothermodynamic methods. The two arrows along the slopes indicate the user’s preference for computational efficiency or flow physics. For example, for conceptual design of a RLV, one needs to apply ZONAIR at the bottom layer. For accuracy in detailed analysis in heat rate prediction, one needs to examine the solutions due to RANS/LAURA [8] and BGK [9] in the upper layer (Fig 3). Further the CFAST pyramid is supported by four kinds of mesh/grid generations: surface panels, structured grids, unstructured grids and a grid free scheme (according to Hui’s unified Lagrangian-Euler coordinate, ULEC, formulation [10]). Next, we will describe methods in each layer of the CFAST pyramid from top down.

Boltzmann/BGK approach

Shown in Table 1 are the Continuum (macroscopic) and Gas-kinetic (microscopic) approaches of CFD methods contained in the CFAST pyramid. The conventional Euler/Navier-Stokes based CFD methods in accord with macroscopic description are only valid in the continuum regime. The gas-kinetic DSMC and direct Boltzmann integration approaches follow the microscopic description and are theoretically valid for the whole flow regime, thereby suitable as a unified methodology.

Flow regimes	Continuum		Transitional	Free Molecule
	$K_n \rightarrow 0$	$K_n < 0.01$	$0.01 < K_n < 1$	$K_n > 1$
<i>Continuum CFD</i> (macroscopic)	Euler	Navier-Stokes	Burnett	
<i>Gas-kinetic CFD</i> (microscopic)	DSMC			
	Boltzmann/BGK			

Table 1 – Valid ranges of CFD flow models vs Flow regimes

However, the use of DSMC and direct Boltzmann solver in the continuum and near-continuum regimes is computationally very costly. For this reason, we turned to the BGK approximation of Boltzmann equation [6] as a first measure. Substantial progress has been made in implementing the gas-kinetic BGK scheme in the mainstream finite-volume CFD framework and generalizing it to account for nonequilibrium flows [9] (e.g., Fig 4-Fig 11).

Continuum CFD Methods

- **CFL3D** [7]: *Euler/thin-layer NS, 2D/3D, steady/unsteady, turbulence models*
Original code is supported by NASA Langley. With support of NSF, we have created highly accurate MVP (Monotonicity/Vorticity-Preserving) reconstruction module to enhance the resolution of fine flow structures such as the vortices, turbulence eddy, and acoustic waves, etc. As one of the leading groups in CFL3D methodology, ZONA is officially a CFL3D commercialization company per ZONA/NASA software release agreement 2002.

- **Unified Lagrangian/Eulerian Coordinates CFD Method [10]:**

ULEC is a “gridless” scheme for high-level CFD methods, in that one can start off an initial grid to proceed with the computation. Since time or artificial time is one of the coordinates, which also representing the flow streamlines, the advantages of ULEC amount to: (i) Sharply resolved slip lines and shocks and (ii) Flow generated grid. ULEC method generates a space marching (steady) solver and a time-marching (unsteady) solver.

Its Space-Marching solver is (i) specific for steady supersonic/hypersonic flows and (ii) Computationally very efficient (typically 1/1000 of the computing time of the time-marching schemes), see Figs 12-13.

Its Time-Marching solver is (i) General for any flow regimes, subsonic/supersonic or mix flow (Fig.14); (ii) Computationally less efficient than the Space-Marching scheme, and (iii) Readily extendable to aeroelastic applications.

POD-Based CFD

However, the low computational efficiency of the above high-level CFD methods would prevent sufficient iterations in the design cycles. On the other hand, the lower-level aerodynamic methods such as ZONAIR are inadequate to accurately predict blunted-nose aerodynamics and lee-side aerodynamics under high angles of attack, among other stringent hypersonic problems. This prompts us to apply the Proper Orthogonal Decomposition (POD) technique to the CFD results and construct an efficient yet accurate Reduced Order Model (ROM) via Response Surface Method (RSM), to compliment the lower-level aerodynamic methods such as ZONAIR, for rapid aerothermodynamic analysis. For a complex geometry such as X-34 at a stringent flow condition, say at high angle of attack, the POD/RSM method could provide accurate CFD solution on the lee-side of the X34 which only requires a few seconds on a PC. Figs. 15-16 show POD/RSM solutions versus direct CFD solutions for X-34.

Hypersonic Panel Method-ZONAIR

ZONAIR is an expedient high-fidelity 3D panel code for rapid design/analysis of very complex wings/bodies. It is an ideal method for rapid conceptual design, for it is a compromise between the computational expediency with solution accuracy among all the methods concerned (see Fig 17). More importantly, it covers the unified subsonic, sonic, supersonic and hypersonic flight regimes. Given flight conditions, it provides aerodynamic pressures/forces/magnitudes generator to efficiently create aerodynamic and loads databases for rigid/elastic bodies, their 6DOF simulation and critical loads identification. ZONAIR is formulated based on the unstructured surface panel scheme that is compatible to the finite element methods. This enables the direct adoption of off-the-shelf finite element pre- and post-processors such as PATRAN, I-DEAS, FEMAP, etc. for ZONAIR panel model generation (see Fig 18). The specific capabilities of ZONAIR are also clearly stated in Fig 18.

ZONAIR consists of many submodules for various disciplines that include (1) AIC matrix generation module, (2) 3-D spline module, (3) Trim module, (4) Aeroheating module, (5) Vortex roll-up module, and (6) Aerodynamic stability derivative module. The interrelationship of ZONAIR with other engineering software systems such as the pre-processor, structural finite element method (FEM), Computational Fluid Dynamics (CFD) method, six degree-of-freedom (6 d.o.f.) and critical loads identification is depicted in Fig 18.

ZONAIR has been under continuous development by ZONA throughout the last decade. Its current version has proven capability accounting for multi-body interference, ground interference, wave reflection and store-separation, aerodynamics in hypersonic/supersonic as well as subsonic

flow domains (Table 1). By comparison, ZONAIR is clearly the best choice as an expedient and versatile aerodynamic methodology. In what follows, we present the results of several hypersonic aerodynamics/aerothermodynamics applications based on ZONAIR and CFL3D [7]. These include:

- CKEM (Compact Kinetic Energy Missile) at $M = 6.0$, $\alpha = 2^\circ$ (Figs 19(a)&(b))
- 15° Blunt Cone at $M = 10.6$ and $\alpha = 5^\circ$ (Figs 20(a)&(b))
- X-34 at $M = 6.0$, $\alpha = 9^\circ$ and altitude = 183 Kft (Figs 21(a)&(b))

TPS Sizing/Optimization

The TPS sizing objective is to minimize the TPS weight while satisfying the thermal protection requirement and the load-carrying requirement of the combined RLV/TPS structure. The developed TPS sizing procedure can be demonstrated by a constructed prototypical TPS/AFRSI (Advanced Flexible Reusable Surface Insulation) model [11] (Figs 22 and 23).

Here we adopt the complex variable differentiation technique to derive the sensitivity of the NASA aerothermal code MINIVER for TPS sizing/optimization procedure (Fig 24). Minimum thicknesses for all six layers of the selected TPS are posed as a part of the constraints. The initial temperature is 100°F and the maximum temperature constraint at the 6th layer (bottom) is 300°F (Fig 24) (Note that each layer has its own maximum temperature constraint posed as well). The complex variable differentiation sensitivity is shown to be superior to that obtained by conventional finite difference method for temperature changes of layer 6 due to a thickness change in layer 3 (Fig 25). With the computed MINIVER sensitivity, TPS optimization can then be carried out by ASTROS, an automated structural optimization tool; the procedure is shown in Fig 26. The final outputs in terms of final (optimized) thickness, temperature and weight for each layer are listed in Fig 27.

In summary, an optimization procedure for TPS weight sizing has been developed using ASTROS optimizer operated on MINIVER by means of an innovative Complex Variable Differentiation-derived sensitivity. The result is a TPS/OPT module. For demonstration, TPS/OPT is applied to a prototypical TPS subsystem with a given heat-flux input at point A of X-43. The optimized total TPS weight is found to be reduced by 30% terminated after the 3rd design cycle, while satisfying all TPS temperature constraints.

References

- [1] Liu, D.D., Chen, P.C., Tang, L., Chang, K.T., Chemaly, A., and Kamhawi, H., "Integrated Hypersonic Aerothermoelastic Methodology for Transatmospheric Vehicle (TAV)/Thermal Protection System (TPS) Structural Design and Optimization," AFRL-VA-WP-TR-2002-3047, 2002.
- [2] Liu, D.D., Chen, P.C., Tang, L., Chang, K.T., "Expedient Hypersonic Aerothermodynamics Methodology for RLV/TPS Design," AIAA paper 2002-5129, 11th AIAA/AAAF International Conference: Space Planes and Hypersonic Systems and Technologies, Sep, 2002, Orleans, France.
- [3] Chen, P.C., Liu, D.D., Tang, L., Chang, K.T., "Hypersonic Aerothermodynamics/Aerothermoelastics Methodology for RLV/TPS Design and Analysis," AIAA paper 2003-0897, 41th AIAA Aerospace Sciences Meeting, Jan, 2003, Reno, Nevada.
- [4] Chen, P.C., Liu, D.D., Tang, L., Chang, K.T., Gao, X.W., "Hypersonic Aerothermodynamics using ZONAIR for RLV/TPS Design and Analysis," Thermal and Fluids Analysis Workshop (TFAWS) 2003, Aug, 2003, ODU center, Hampton, Virginia.

- [5] Chen, P.C. and Liu, D.D. "Unified Hypersonic/Supersonic Panel Method for Aeroelastic Applications to Arbitrary Bodies," *Journal of Aircraft*, Vol. 39, No. 3, May-June 2002.
- [6] Bhatnagar, P.L., Gross, E.P., and Krook, M., "A Model for Collision Processes in Gases. I. Small Amplitude Processes in Charged and Neutral One-Component Systems," *Physical Review*, Vol. 94 (1954), pp.511.
- [7] Krist, S.L., Biedron, R.T. and Rumsey, C.L., "CFL3D User's Manual Version 5.0," NASA Langley Research Center, Hampton, VA, 1997.
- [8] Cheatwood, F.M., Gnoffo, P.A., "User's Manual for the Langley Aerothermodynamic Upwind Relaxation Algorithm (LAURA)," NASA-TM-4674, April 1996.
- [9] Tang, L., and Xu, K., "Unified Gas-Kinetic Computational Algorithm for Continuum and Rarefied Flows," AIAA-2004-1179, 2004.
- [10] Hui, W.H., and Tang, L., "A Unified Coordinates Approach to Computational Fluid Dynamics," AIAA-2003-4239, 2003.
- [11] Myers, D.E., Martin, C.J., and Blosser, M.L., "Parametric Weight Comparison of Advanced Metallic, Ceramic Tile, and Ceramic Blanket Thermal Protection Systems," NASA-TM-2000-210289.

ZONAIR in HYAAT

Hypersonic Aerodynamic Aerothermoelastics for TPS program

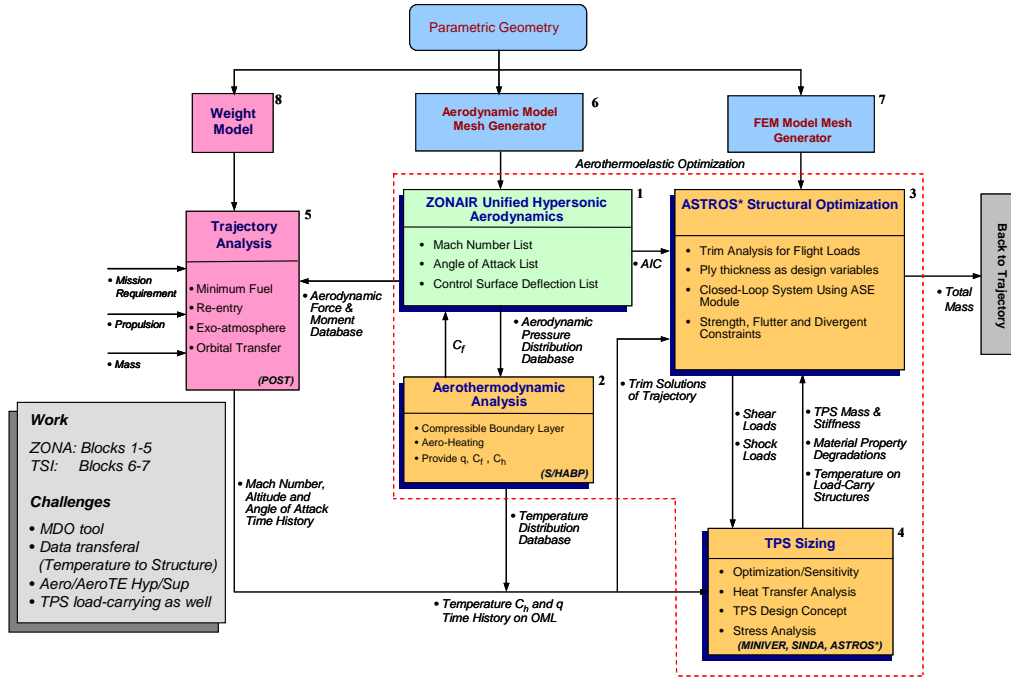


Fig. 1 HYAAT software system

ZONA CFD/POD Module in HYAAT

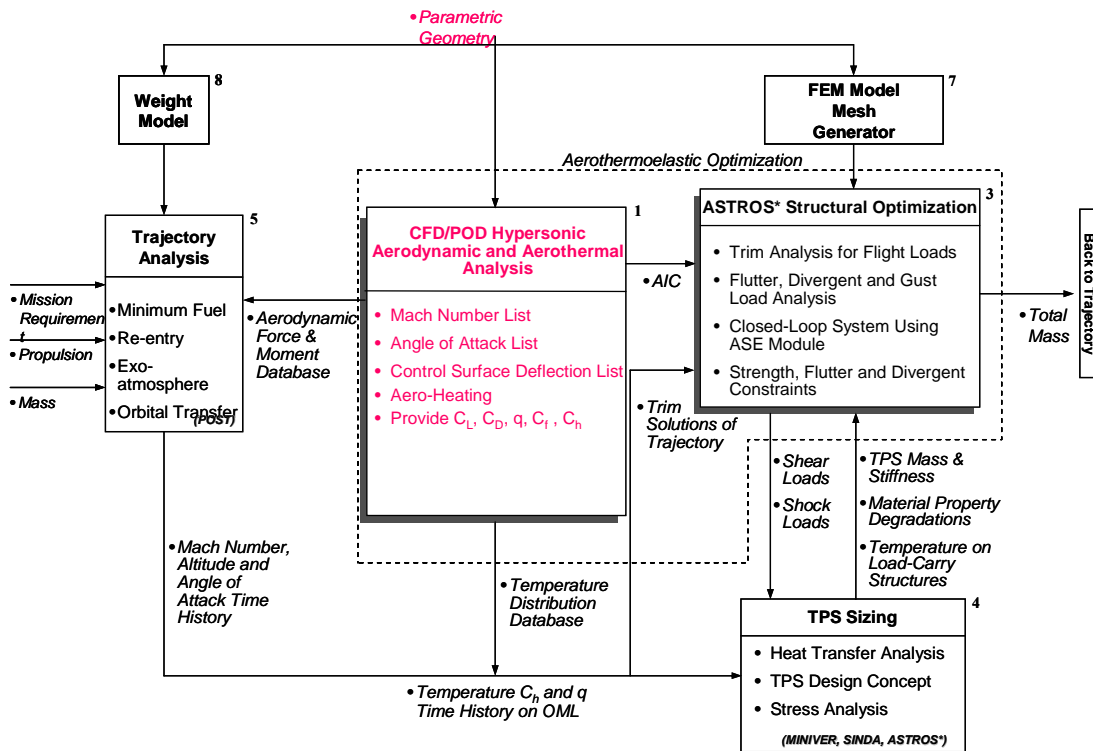


Fig. 2 ZONA CFD/POD module in HYAAT system

ZONA Fluid/Aerothermo-dynamics Software Toolbox (FAST)

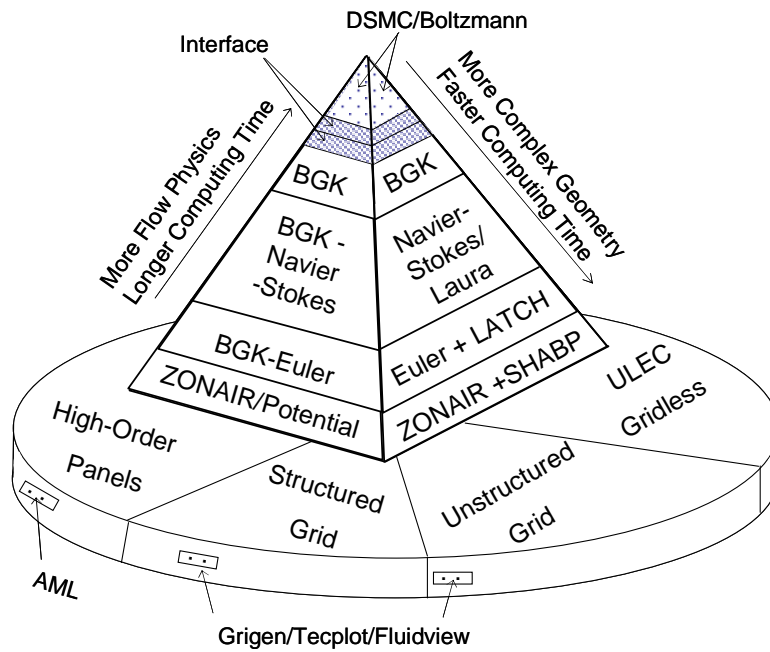


Fig.3 CFAST software system

ZONA BGK Computational Tool (4)

Case 1. Hypersonic flow passing a cylinder (NASA TM-100484)

- Demonstrate superior accuracy of BGK scheme
- $M_\infty=8.03$, $Re=1.835 \times 10^5$, $T_\infty=124.94^\circ\text{k}$, $T_W=294.44^\circ\text{k}$
- 63x35 points
- $Re_c=50$ based on the first mesh size away from wall

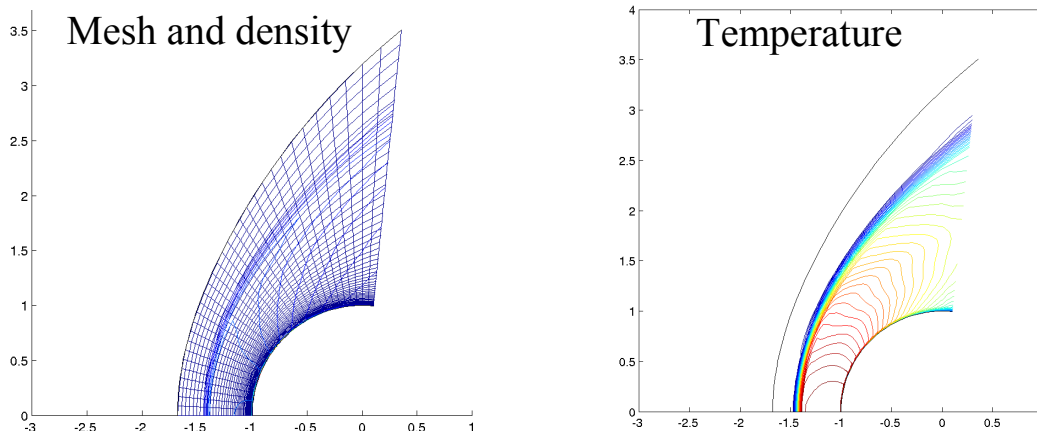


Fig.4

ZONA BGK Computational Tool (5)

Surface pressure and heat transfer distribution

- Both BGK-NS and CFL3D predict reasonable surface pressure distribution – inviscid phenomenon
- BGK-NS predicts reasonable heat transfer on surface whereas CFL3D overpredicts more than 3 times
- Poor grid resolution in boundary layer is forgiving for BGK-NS but not CFL3D

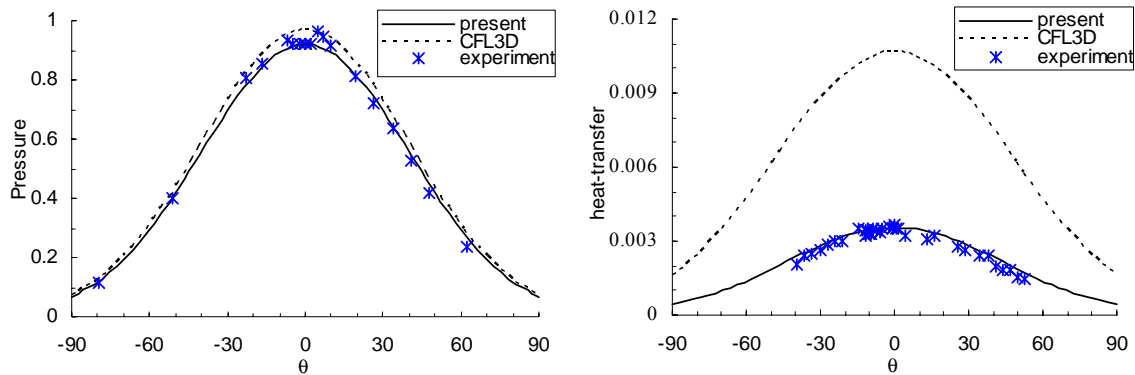


Fig.5

ZONA BGK Computational Tool (6)

Case 2. Type IV shock interaction (NASA TM-100484)

- Demonstrate superior accuracy of BGK scheme
- $M_\infty=8.03$, $Re=1.94 \times 10^5$, $T_\infty=122.11^\circ\text{k}$, $T_W=294.44^\circ\text{k}$
- Incident shock position: $y=0.3271x+0.4147$
- 181×101 points
- CFL3D fails to produce a converged solution

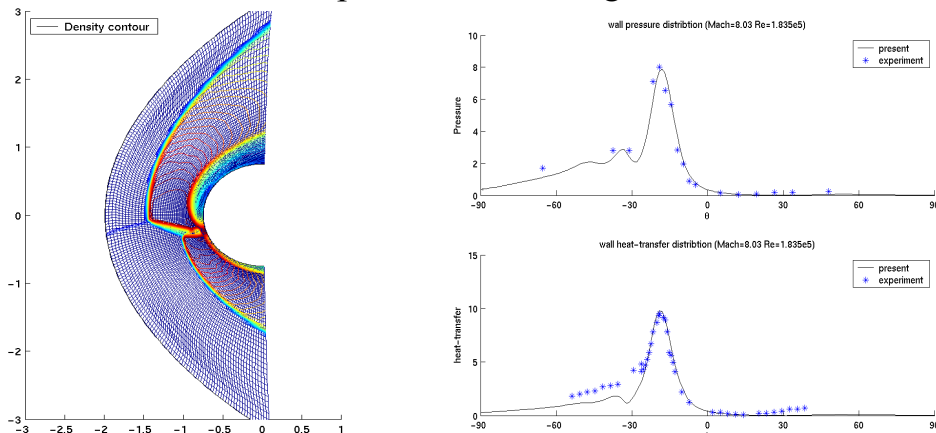


Fig.6

ZONA BGK Computational Tool (7)

Case 3. Double cone case (Run 28 in AIAA-2003-3641)

- Demonstrate superior accuracy of BGK scheme
- $M_\infty=9.59$, $Re=13090$, $T_\infty=185.56^\circ k$, $T_W=293.33^\circ k$
- 500x200 points
- CFL3D fails to produce a converged solution

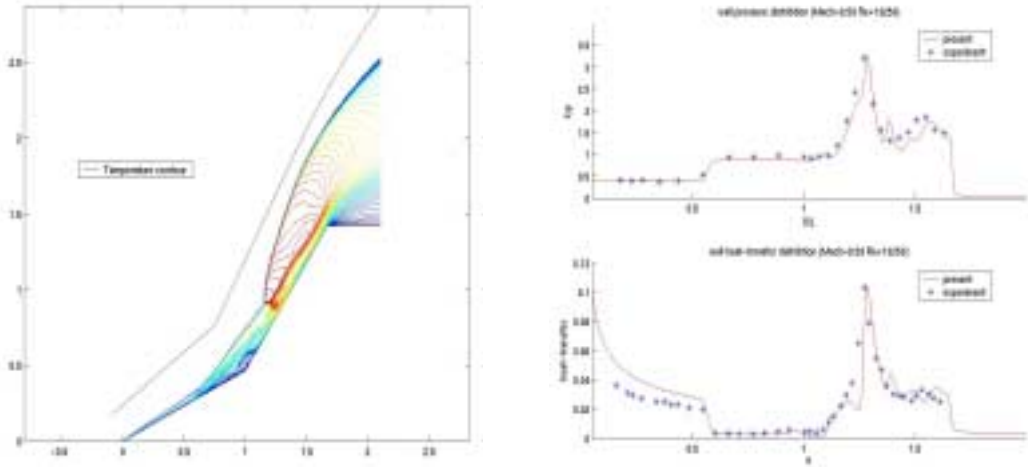


Fig.7

ZONA BGK Computational Tool (8)

Case 4. Alsmeyer nitrogen shock structure (JFM 1976)

- Demonstrate the feasibility of using BGK scheme for thermal non-equilibrium flow simulation
- See strong non-equilibrium effect
- See little rarefaction effect
- Equilibrium BGK-NS:

$$g = \rho \left(\frac{\lambda}{\pi} \right)^{\frac{5}{2}} e^{-\lambda [(u-U)^2 + v^2 + w^2 + \xi_1^2 + \xi_2^2]}$$

$$\int (g - f) \psi d\Xi = S = (0, 0, 0, 0)^T$$

Non-equilibrium BGK-NS:

$$g = \rho \left(\frac{\lambda_T}{\pi} \right)^{\frac{3}{2}} \left(\frac{\lambda_R}{\pi} \right) e^{-\lambda_T [(u-U)^2 + v^2 + w^2] - \lambda_R (\xi_1^2 + \xi_2^2)} \int (g - f) \psi d\Xi = S = \left(0, 0, 0, \rho \frac{\mathcal{E}_R^* - \mathcal{E}_R}{Z_R \tau_c} \right)^T$$

Non-equilibrium BGK-Xu: $\tau \rightarrow \tau_*$

- $Z_R=4$

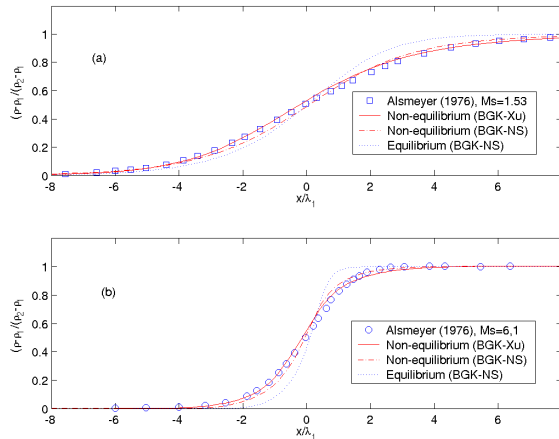


Fig.8

ZONA BGK Computational Tool (9)

- $M_\infty=11$ case ($Z_R=5$)

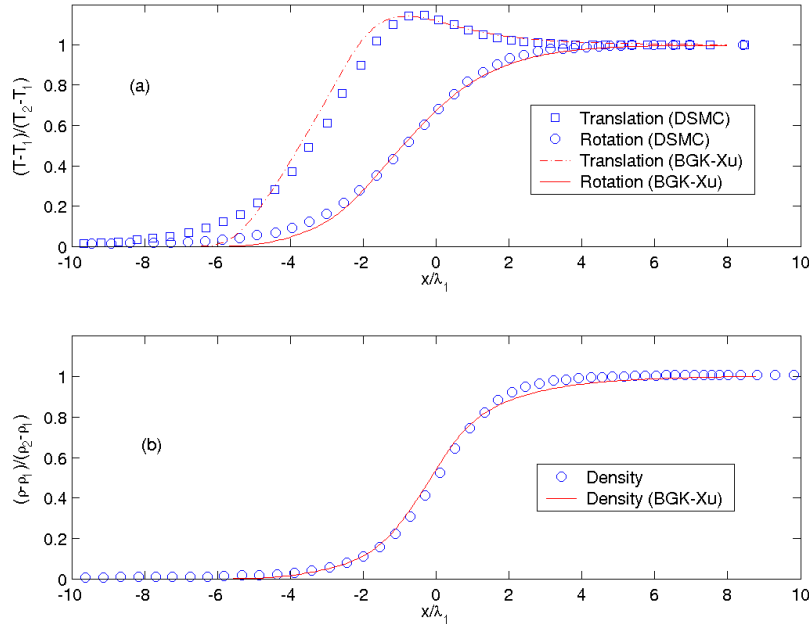


Fig.9

ZONA BGK Computational Tool (10)

Case 5. Kewley & Hornung nitrogen shock dissociation (Chemical Physics Letters, 1974)

- Demonstrate the feasibility of using BGK scheme for chemical non-equilibrium flow simulation

- $\rho_1=0.0467 \text{ kg/m}^3$,

$u_1=4800 \text{ m/s}$,

$p_1=4133 \text{ N/m}^2$

- Non-equilibrium

BGK-NS:

$$f_t^{(N_2)} + u f_x^{(N_2)} = (g^{(N_2)} - f^{(N_2)}) / \tau$$

$$f_t^{(N)} + u f_x^{(N)} = (g^{(N)} - f^{(N)}) / \tau$$

$$\sum_{s=1}^5 \int (g^{(s)} - f^{(s)}) \psi^{(s)} d\Xi^{(s)} = S = (\dot{W}^{(N_2)}, \dot{W}^{(N)}, 0, -\dot{W}^{(N)} h_0^{(N)}, \rho^{(N_2)} \frac{\mathcal{E}_V^{(N_2)*} - \mathcal{E}_V^{(N_2)}}{\langle \tau^{(N_2)} \rangle} + \dot{W}^{(N_2)} \mathcal{E}_V^{(N_2)})^T$$

$$g^{(N_2)} = \rho^{(N_2)} \left(\frac{\lambda_T^{(N_2)}}{\lambda_V} \right)^{\frac{5}{2}} \left(\frac{\lambda_V}{\lambda_T} \right)^{\frac{K_V}{2}} e^{-\lambda_T^{(N_2)} [(u-U^{(N_2)})^2 + \xi^2] - \lambda_V \eta^2}$$

$$g^{(N)} = \rho^{(N)} \left(\frac{\lambda_T^{(N)}}{\lambda_V} \right)^{\frac{3}{2}} e^{-\lambda_T^{(N)} [(u-U^{(N)})^2 + \xi^2]}$$

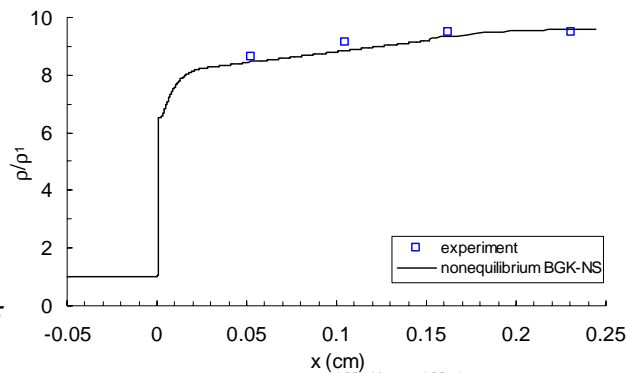


Fig.10

ZONA BGK Computational Tool (11)

Case 6. Cylinder case (AIAA-01-2962)

- Demonstrate the validity Kn range of BGK scheme
- With slip b.c. only, BGK-NS already matches the test data up to $Kn=0.8$

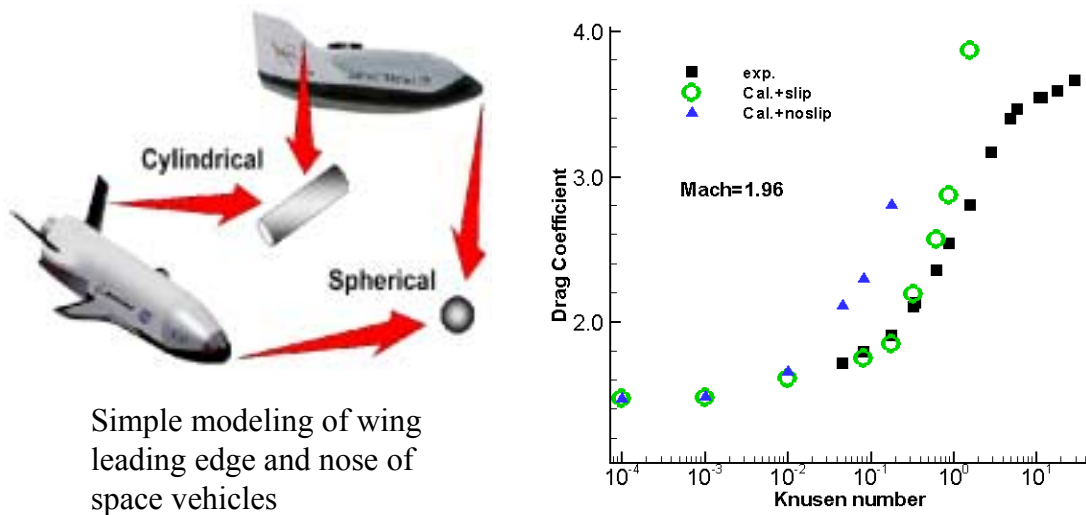


Fig. 11

Flow past a thin concave body of $y=(\tan 3^\circ)x+0.0476x^2$ ($M_\infty=15$)

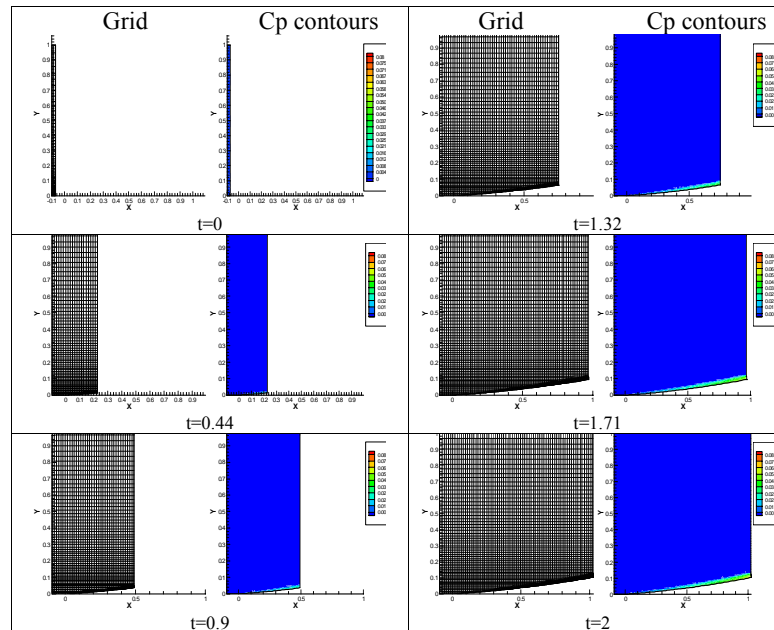


Fig.12

Channel flows ($M_\infty=1.8$)

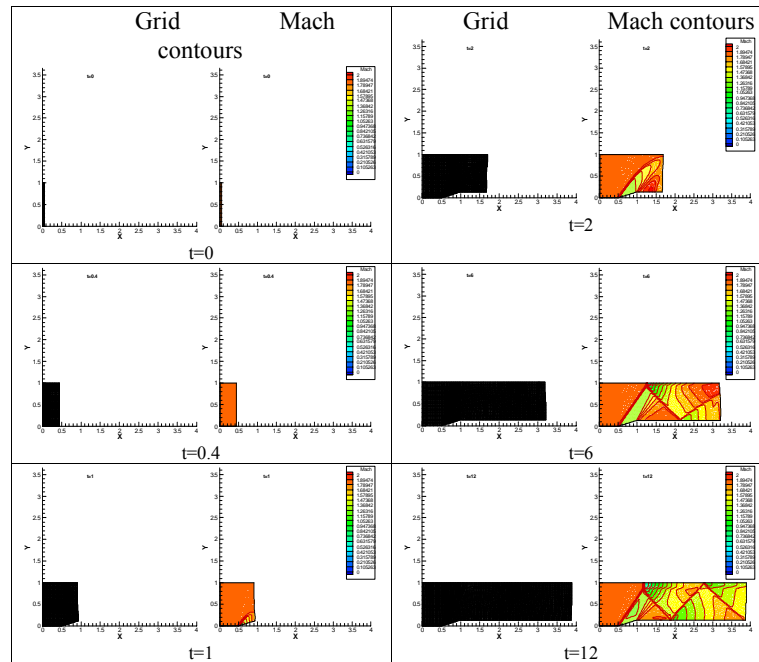


Fig.13

Cp contours of a thick concave body of $y=(\tan 35^\circ)x+0.3x^2$ ($M_\infty=15$)

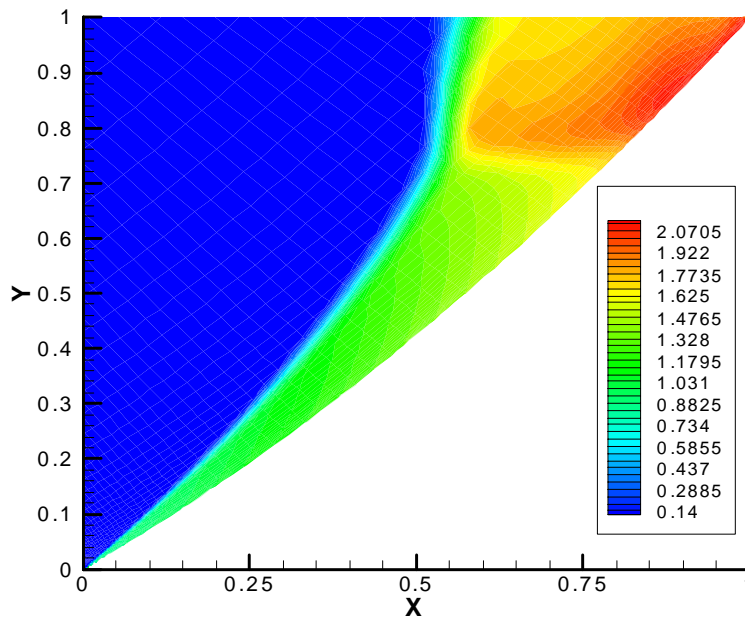


Fig. 14

Proper Orthogonal Decomposition (1)

- CFD solutions vs. POD reconstruction with 3 modes ($M_\infty=2$)

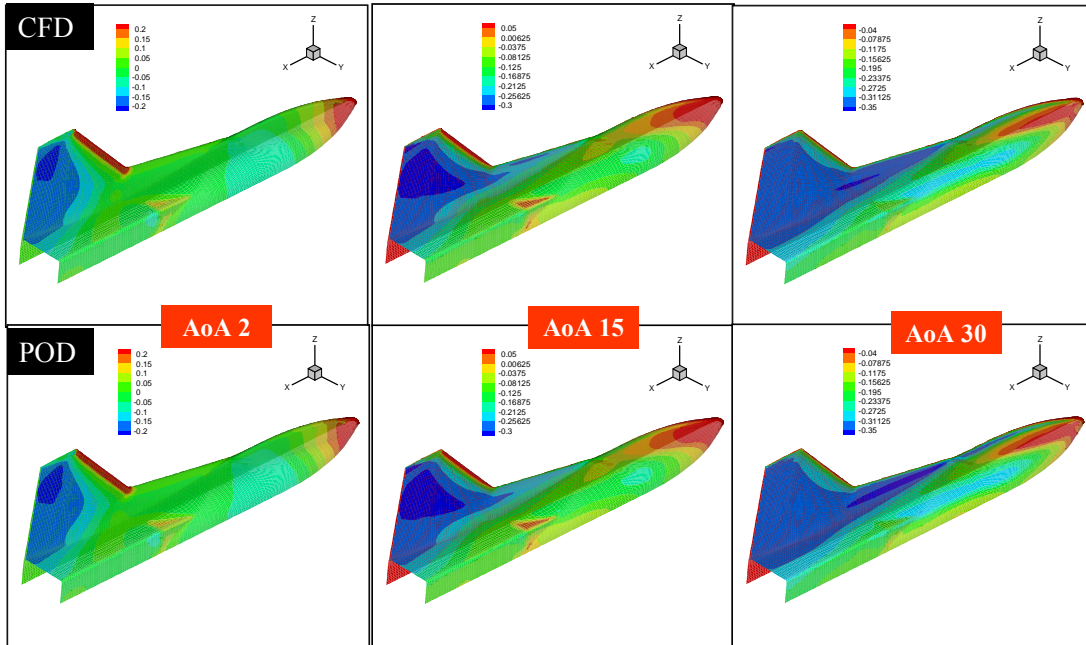


Fig. 15

Proper Orthogonal Decomposition (2)

- CFD solutions vs. POD reconstruction with 3 modes ($M_\infty=10$)

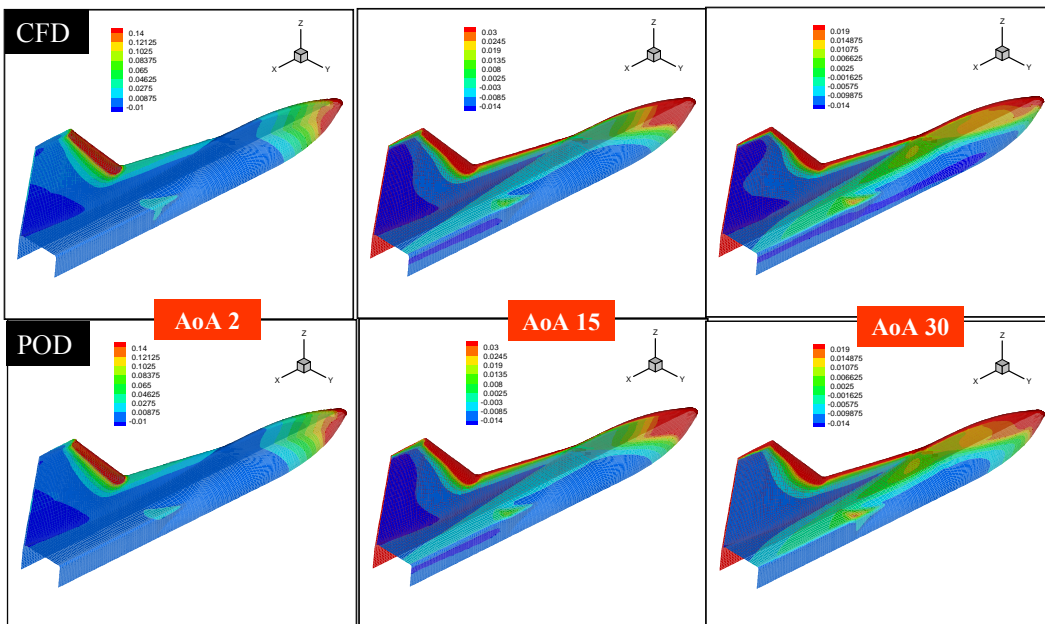


Fig.16

ZONAIR Capability vs Other Aerodynamic Codes

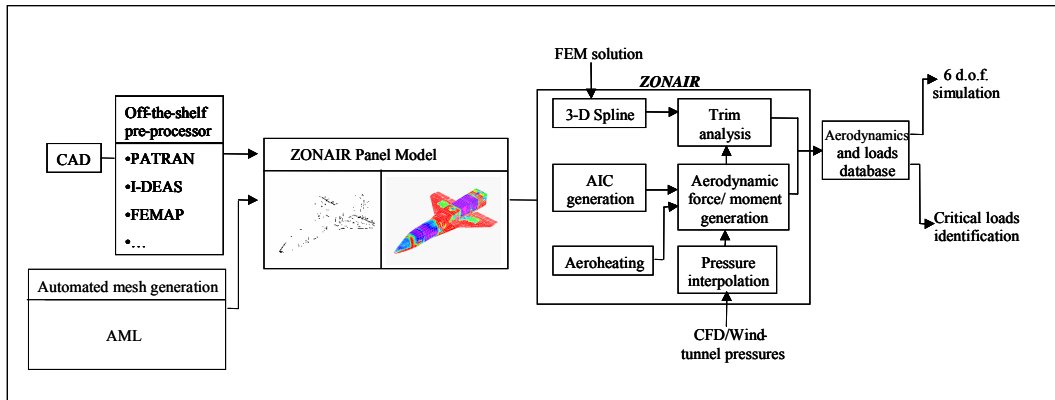
ZONAIR is a versatile tool for rapid aerodynamic database generation

- Aerodynamic AIC matrix readily coupled with FEM
- Force/moment coefficients
- Multi-body interference aerodynamics
- Accurate aerodynamics for aeroheating prediction

Code	Method	Computational Efficiency	Streamline Solution for Aeroheating	Hypersonic/Supersonic/Subsonic Mach No.	AIC for Structural FEM	Geometry High Fidelity	High AOA	2 Body Aero Interference
<i>CFD3D</i>	Euler/N-S	30 hrs/ X-34	Yes	All	No	Yes	Yes	Yes
<i>PANAIR</i>	Potential	20 min/ X-34	No	Supersonic/ Subsonic	No	Yes	No	Yes
ZONAIR	Potential + PEF	20 min/ X-34	Yes	All	Yes	Linear-Order Panel	Yes	Yes
<i>ZAERO</i>	Potential + PEF	10 min/ X-34	Yes	All	Yes	Constant Order Panel	No	Yes
<i>APAS</i>	Potential + Empirical	<10 min	Newtonian S.L.	Empirical for hypersonics	No	Low-Order Panel	No	Yes
<i>MINIVER</i>	Analytical/ Empirical	<<10 min	No	No subsonics	No	No	No	No
<i>DATCOM</i>	Analytical/ Empirical	<< 10 min	No	All	No	No	Yes	No
<i>AP98</i>	Analytical/ Empirical	<< 10 min	No	All	No	No	Yes	No

Fig.17

ZONAIR and Interfacing Capability w/ other Softwares



- Unified high-order subsonic/supersonic/hypersonic panel methodology
- Aerodynamic influence coefficient (AIC) matrix for rapid data retrieval
- Unstructured surface panel scheme compatible to the finite element method
- Rapid panel model generation using COTS/FEM pre- and post-processors
- Accurate streamline solution with axisymmetric analogy for aerothermodynamics
- Trim module for flexible loads and aeroheating module for TPS design/analysis
- Multibody interference/separation aerodynamics
- Pressure interpolation scheme for transonic flexible loads generation
- Aerodynamic database for 6 DOF simulation and critical loads identification

Fig. 18

Pointed-Nose CKEM Body: Aerodynamics

$M_\infty = 6.0, \alpha = 2^\circ$

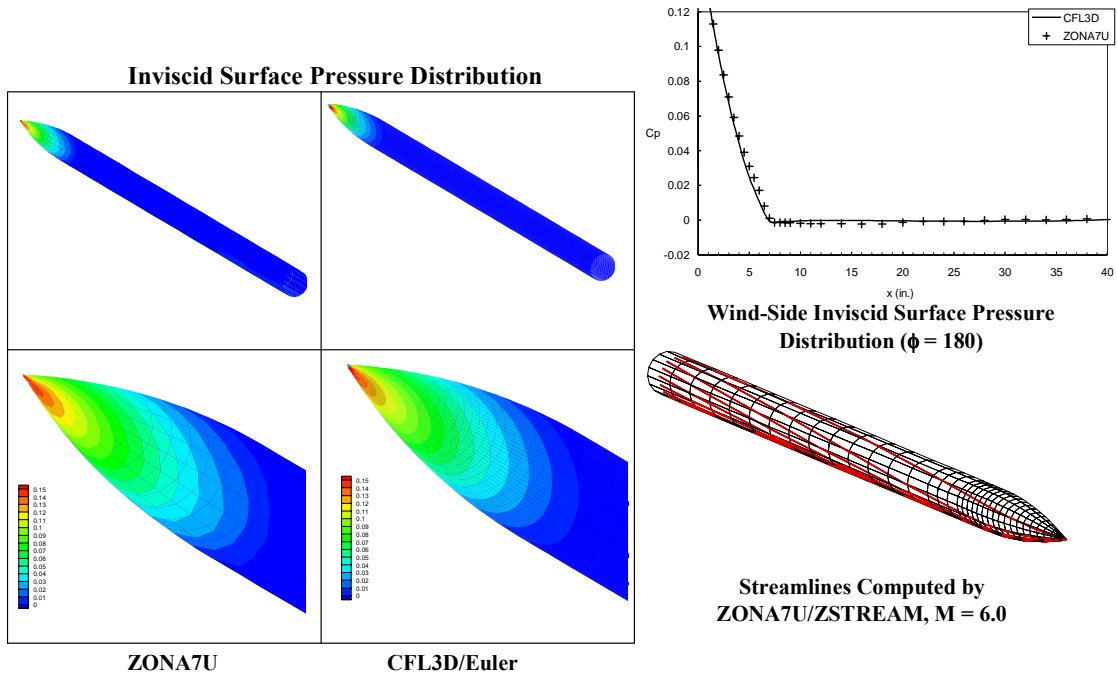


Fig. 19(a)

Pointed-Nose CKEM Body: Aerodynamics

$M_\infty = 6.0, \alpha = 2^\circ, P_\infty = 2.66 \text{ psf}, T_\infty = 89.9^\circ\text{R}, T_w = 540^\circ\text{R}$

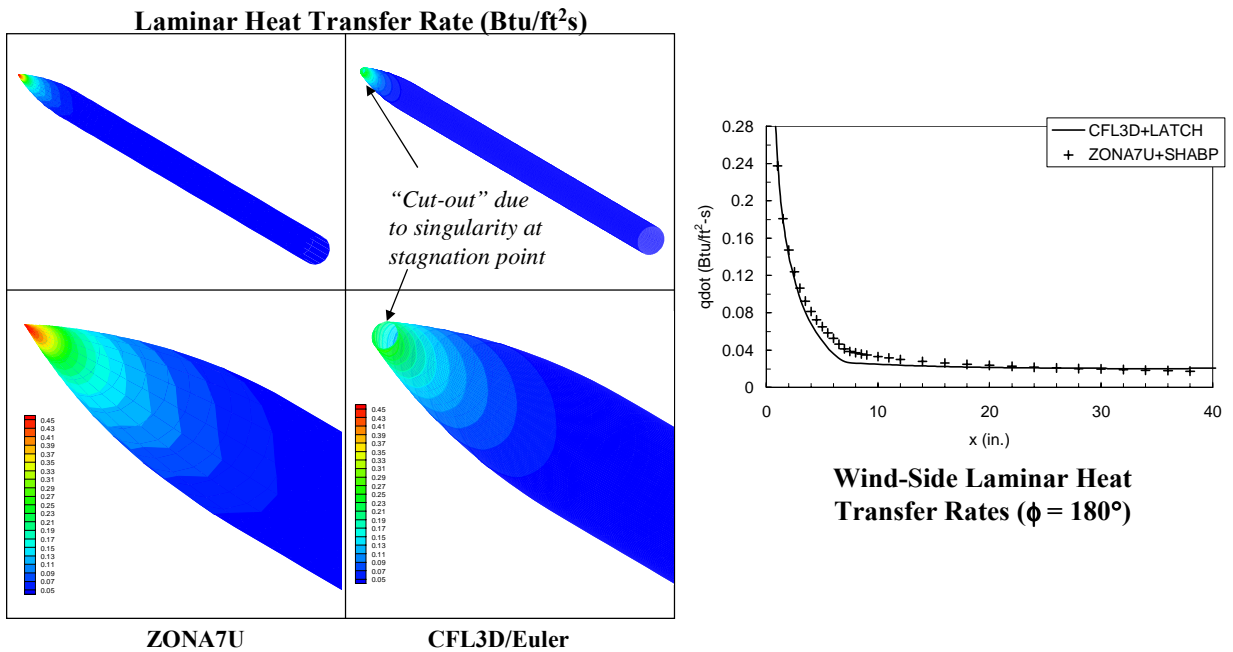


Fig. 19(b)

15° Blunt Cone: Aerodynamics

$M = 10.6, \alpha = 5^\circ$

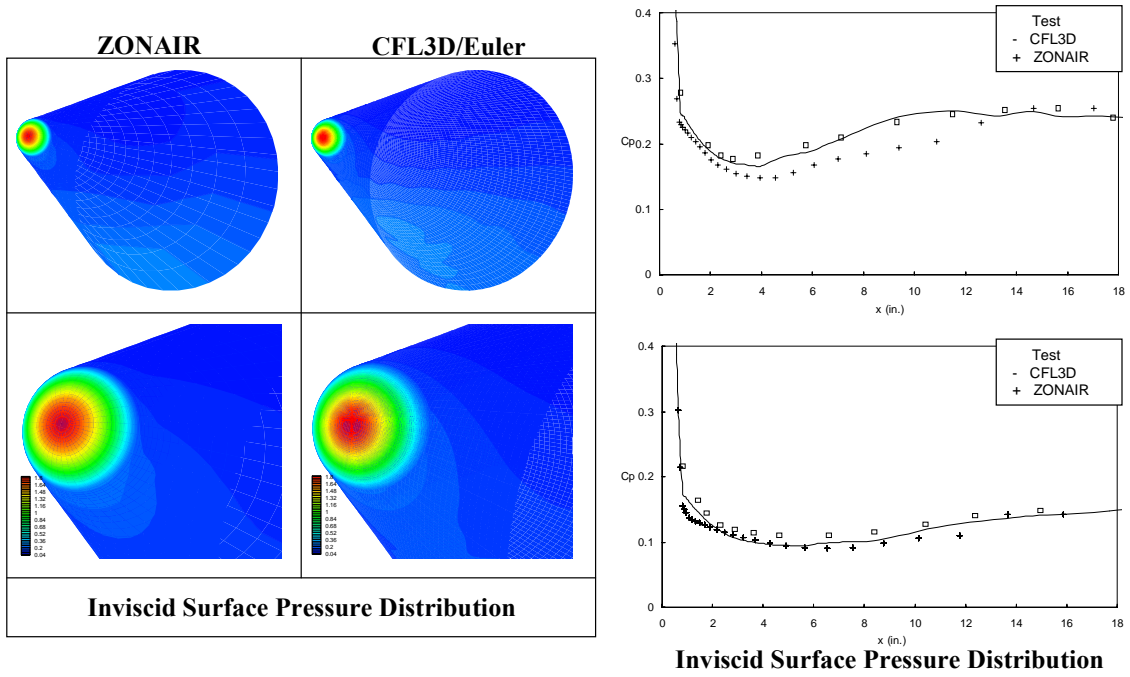


Fig.20(a)

Laminar Heat Rate: 15° Blunt Cone

$M_\infty = 10.6, \alpha = 5^\circ, P_\infty = 2.66 \text{ lb/ft}^2, T_\infty = 89.971^\circ\text{R}, T_w = 540^\circ\text{R}$

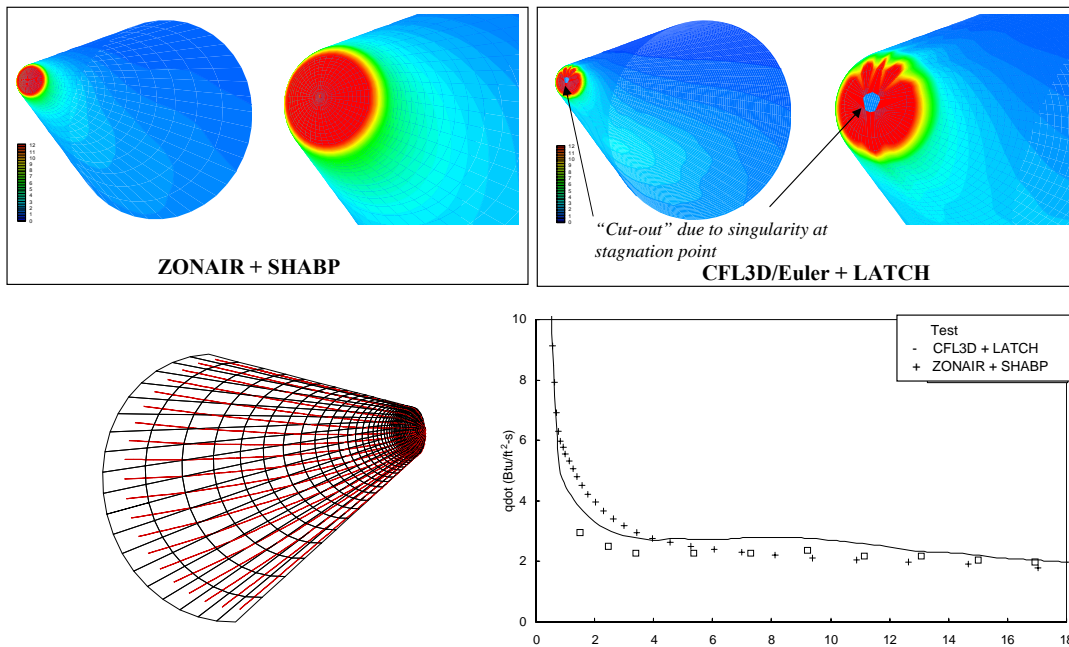


Fig. 20(b)

X-34 Wing-Body: Aerodynamics

$M_\infty = 6.0, \alpha = 15.22^\circ$

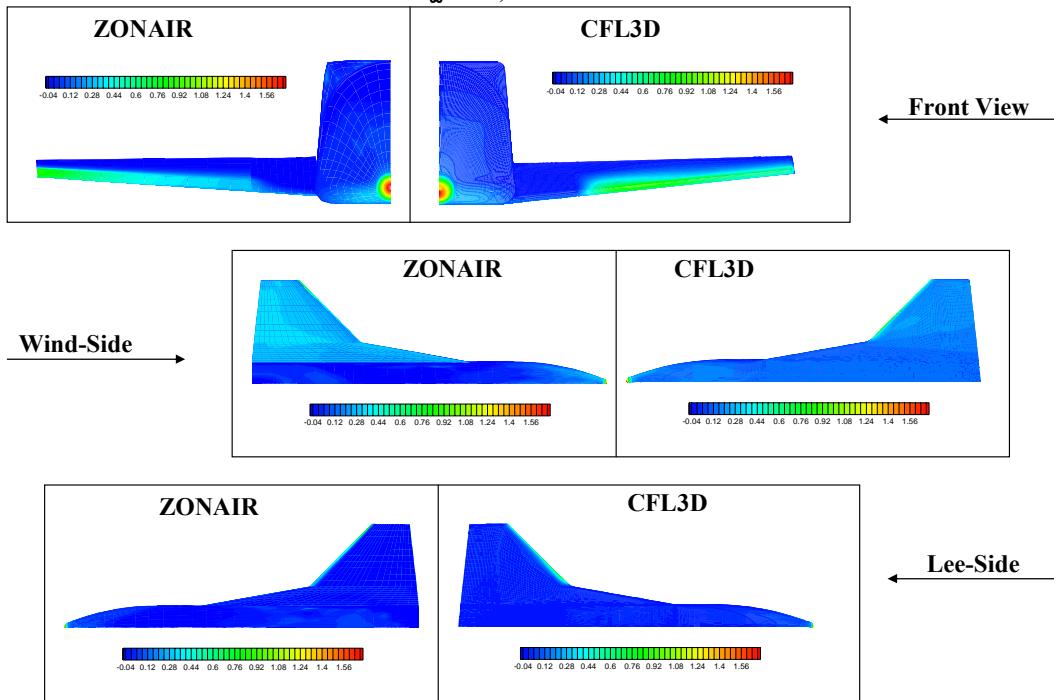


Fig.21(a)

Aeroheating of X-34

$M_\infty = 6.0, \alpha = 15.22^\circ, h = 112 \text{ Kft.}, \text{ Hot Wall, Emissivity} = 0.8, \text{ Turbulent}$

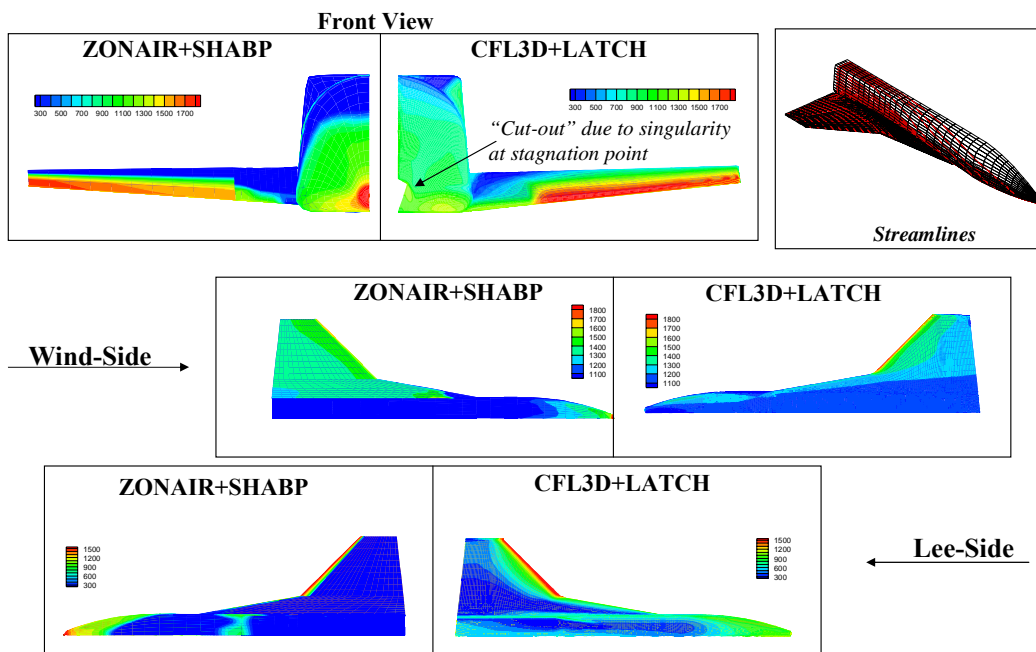
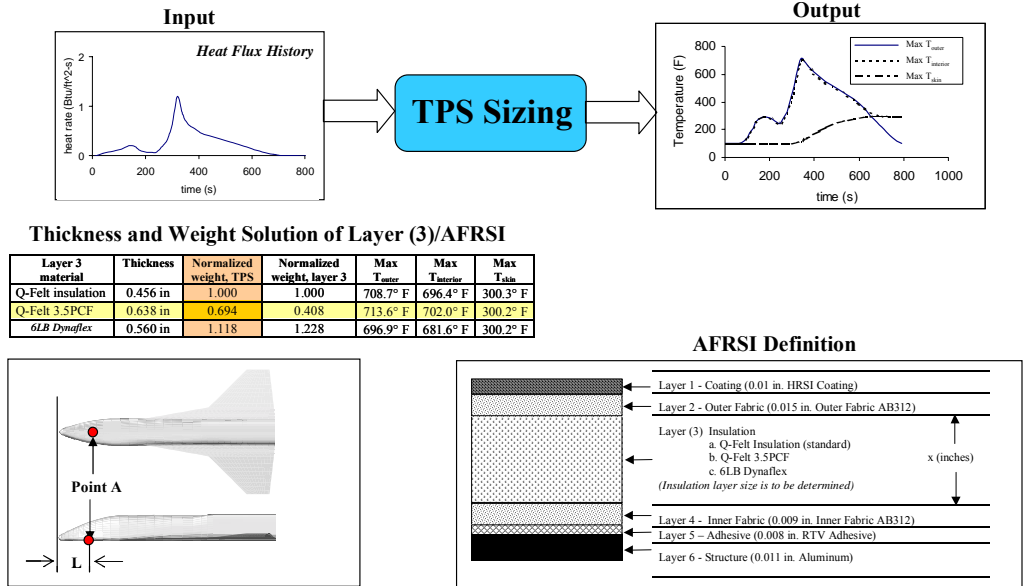


Fig.21(b)

Elementary TPS Sizing of AFRSI

- TPS element selected on windward centerline of X-34 (point A @ L = 50'')
- Heat Rate Input provided by ZONAIR+SHABP from trajectory/aeroheating
- Minimum TPS weight obtained by MINVER/EXITS



* T_{outer} and $T_{interior}$ are the temperatures at the outer edge and (1) to (5) interior layers of the TPS. T_{skin} is the temperature at the nodes within the skin layer 6.

Fig.22

Development of an Optimization Procedure for TPS Sizing (I)

Description of the selected test case

- A six layer TPS system is selected as the test case
- Heat flux time history is obtained from windward side of X-34 centerline.

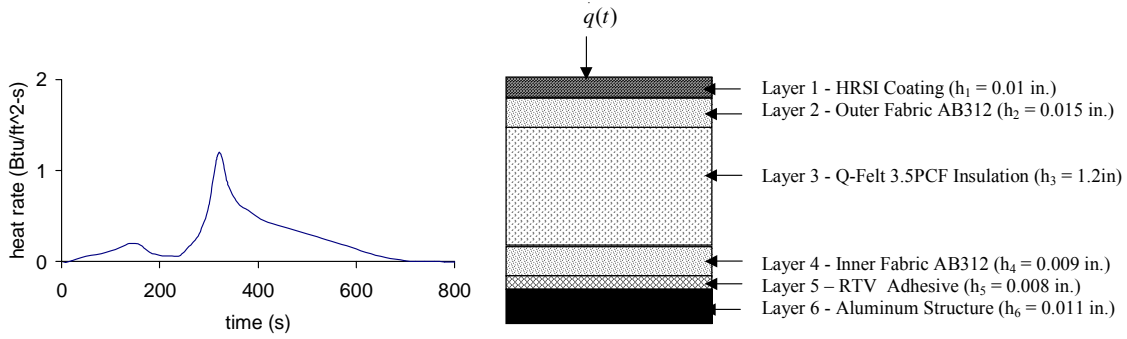
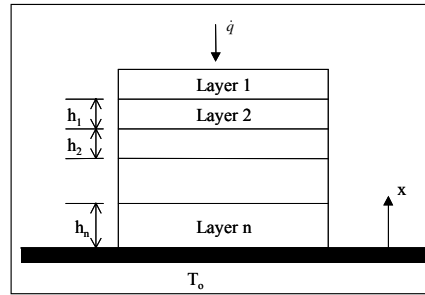


Fig. 23

TPS Sizing Optimization Using Complex-Variable Differentiation Sensitivity

- TPS sizing will be automated by developing an optimization driver of the MINIVER/EXITS code.
- For a given heat flux \dot{q} applied on the outer boundary, the objective is to minimize the total weight of the TPS system while keeping the temperature at each layer (T_i) below their respective maximum operational temperature, T_{oi} .
- Minimize: $W = \sum_{i=1}^n \rho_i h_i$ where ρ_i is the density of the i^{th} layer.
 Subjected to: $T_i < T_{oi} \quad i = 1, 2, \dots, n$
 Design variables: $h_i > 0 \quad i = 1, 2, \dots, n$
- The complex-variable differentiation can provide “numerically exact” derivatives of a complicated function.
 - The variable h of a real function $T(h)$ is replaced by $h + i\Delta h$.
 - For small Δh : $T(h + i\Delta h) = T(h) + i\Delta h \frac{\partial T}{\partial h} + \dots$ Yields: $\frac{\partial T}{\partial h} = \frac{\text{Im}(T(h + i\Delta h))}{\Delta h} + O(\Delta h^2)$
- To incorporate the complex variable technique into the MINIVER/EXITS module for sensitivity analysis is straightforward simply by declaring all variables in the MINIVER/EXITS module as complex variables.
 - The imaginary part of the thickness input of MINIVER/EXITS represents a small incremental thickness.
 - The sensitivity is the imaginary part of the temperature output divided by the incremental thickness.



Typical TPS Sizing Problem

Fig.24

Development of an Optimization Procedure for TPS Sizing (II)

Validation of complex variable differentiation for sensitivity

- Temperature change at Layer 6 due to the change of thickness of layer 3 ($\partial T_6 / \partial h_3$) is computed using both the Complex Variable Differentiation (CV) and the Finite Difference (FD) techniques.
- In order to demonstrate the robustness of the CV, $\Delta h_3 = 10^{-30}$ (near machine zero) is assigned for the CV technique whereas Δh_3 for the FD technique varies from 10^{-2} to 10^{-6} .
- Results show that the accuracy of the FD technique depends on Δh_3 but the CV technique does not.

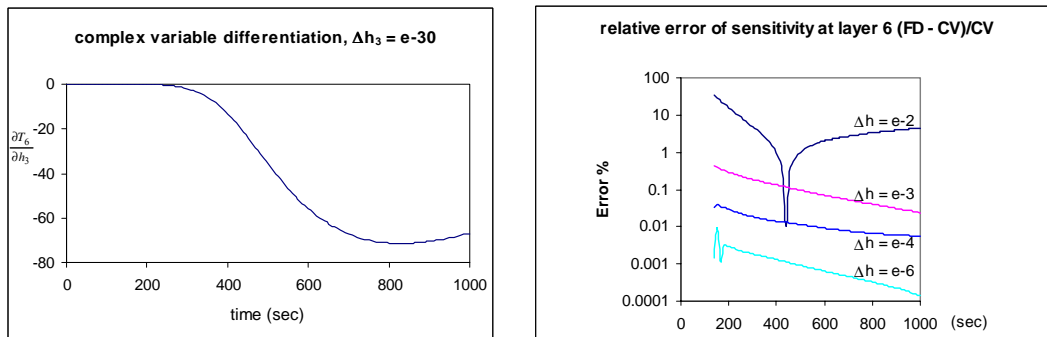


Fig.25

TPS Optimization using MINIVER/OPT

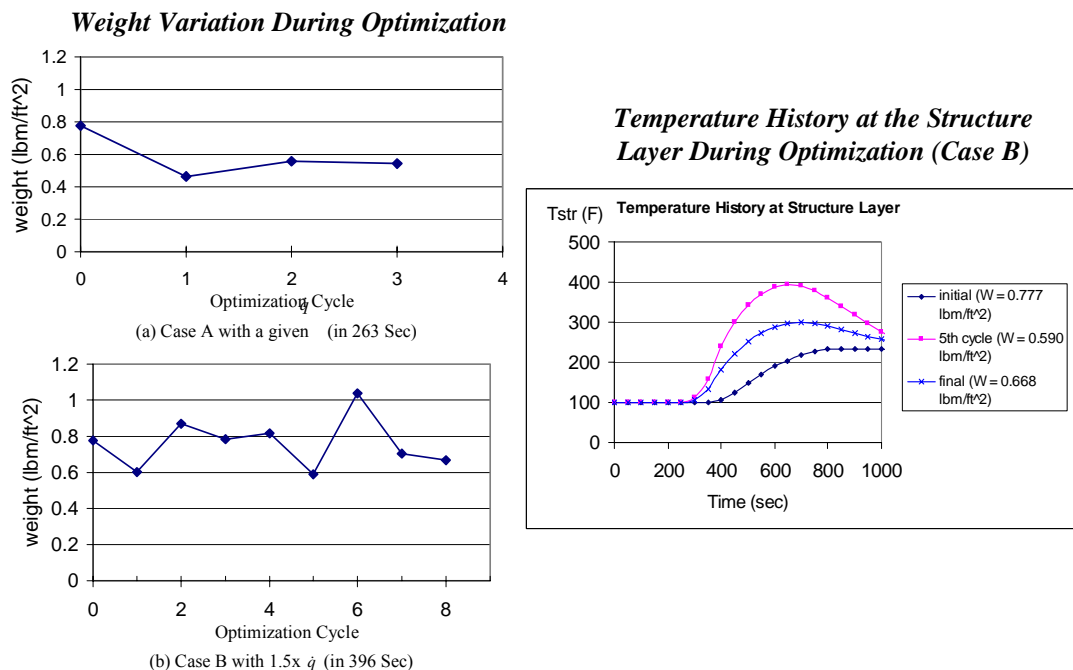


Fig.26

Development of an Optimization Procedure for the TPS Sizing (III) Optimization Results with upper bound = 1.0”

- All design variables reduce to the minimum thickness (0.0072”) except layer 3 ($h_3 = 0.68496$ ”).
- The total weight is reduced from the initial weight = 0.777 lbs/ ft² to the final weight = 0.54256 lbs/ft²

Layer	Material	Temp Limit (°F)	Density (lbm/ft ³)	Specific Heat (But/lbm °F)	Initial Thickness (in)	Max Temp in the Layer (°F)	Optimized Design (in)
1	HRSI Coating	2300	104	0.20	0.01	705.2	0.0072
2	AB312 Fabric	2040	61.5	0.166	0.015	704.9	0.0072
3	Q-Felt	1800	3.5	0.1875	1.2	701.6	0.68496
4	AB312 Fabric	2024	61.5	0.166	0.009	300.0	0.0075
5	RTV-560	550	88	0.285	0.008	300.0	0.0072
6	Aluminum	300	173	0.22	0.011	300.0	0.011

Note: For structure layer (6), thickness is not a design variable.
upper bound thickness = 1.0 in, lower bound = 0.0072 in with original heat flux of X1004601 trajectory

Fig.27